



Preparation, characterization, and Ce(III) adsorption performance of poly(allylamine)/silica composite

Sen Zhou, Xujian Li, Yongjuan Shi, Aref Alshameri, Chunjie Yan*

Faculty of Materials Science and Chemistry, China University of Geosciences, Wuhan 430074, P.R. China, Tel. +86 027 67884283; Fax: +86 027 67884283; emails: zhouseneric@163.com (S. Zhou), 270386005@qq.com (X. Li), 582052143@qq.com (Y. Shi), 2586780906@qq.com (A. Alshameri), chjyan2005@126.com (C. Yan)

Received 22 December 2013; Accepted 7 July 2014

ABSTRACT

In the present work, an organic–inorganic hybrid composite (poly(allylamine)/silica) was facilely prepared through grafting poly(allylamine) onto the modified silica. Surface property, morphology, and texture parameters of the composite were characterized by infrared spectroscopy (FTIR), scanning electron microscopy, and N_2 adsorption/desorption measurements, respectively. Then, the adsorptive property of this composite for recovery of Ce(III) was investigated systematically. Batch tests were performed under a range of conditions to examine the effects of contact time, adsorbent amount, initial Ce(III) concentration, and solution pH. At optimal experimental conditions, the maximum adsorption capacity of Ce(III) was up to 111.8 mg g^{-1} . Full kinetic and thermodynamic investigations as well as isotherm analysis were also undertaken. It was found that the adsorption kinetics could be well fitted by the pseudo-second-order model, whereas the Freundlich model provided the better description for the equilibrium data. The adsorption process was spontaneous and endothermic with an increase of randomness at the solid–solution interface during adsorption. Moreover, the reusability of poly(allylamine)/silica composite was evaluated, and the result showed that the composite could be well reused in several cycles without significant deterioration in its original performances.

Keywords: Silica; Poly(allylamine); Adsorption; Cerium

1. Introduction

Rare earth elements (REEs) are widely distributed across the world and play a vital role in manufacture of tanks, aircrafts, missile steel, aluminum alloy, magnesium alloy, and titanium alloy. Also, they are used as lubricant in electronic, laser, nuclear industry, superconducting, and so many high-techs [1]. Unfortunately, in the processes of exploration and/or processing of REEs, a huge amount of REEs-contained mine

wastewater has been directly discharged [1,2]. Thus, it is highly desirable to seek effective and efficient techniques for recovery of RREs from mine wastewater.

Many technologies have been proposed to recover RREs from mine wastewater. Pietrelli et al. [3] utilized a leaching step with sulfuric acid solutions after filtration and rare earth were precipitated from the leach liquor with adding NaOH. Europium was recovered by precipitation as insoluble EuSO_4 after the reduction of the trivalent species to the divalent state [4]. Gadolinium and samarium were separated and purified

*Corresponding author.

from further solvent extraction stages [5]. Ion exchange using polymeric resins and solvent extraction has become the most useful procedure for extraction and separation of REEs. However, the resins are always broken easily during ion exchange and the eluting process with strong acid [6].

Silica is one of the most common inorganic materials, which has been frequently used as adsorbent for adsorptive purpose. Noticeably, silica can effectively overcome the drawback of resin in mechanical strength [7,8]. Nevertheless, the adsorption capacity of pure silica is generally low because of the evident lack of adsorption sites on its surface. To overcome this problem, a good strategy is to immobilize functional polymer on silica surface. Among various silica–polymer composites, silica polyamine composite is relatively fresh and has been used very recently in the successful recovery and removal of transition metals or precious metals from diverse waste streams and mining leaches [9]. This composite material has many obvious advantages including improved mechanical and chemical stability, higher operational temperatures, and improved mass transfer kinetics [10]. Generally, the silica polyamine composite is composed of a silica core and a polyamine shell [11]. The polyamine layer can be further functionalized with specific ligands to yield a novel organic/inorganic hybrid chelating material [12].

The main purpose of this research, therefore, is to develop a kind of polyamine/silica composite as the adsorbent to recover Ce(III), and disclose the effects of various operational parameters on the adsorption efficiency. In addition, theoretical aspects of such adsorption process such as adsorption isotherm, kinetics, and thermodynamics will be investigated. The reversibility and reusability, effect of competing ions in sorption, and intra-series adsorption behavior of lanthanide element about the material were also investigated.

2. Experimental

2.1. Chemicals

Poly(allylamine), cerium nitrate, hydrochloric acid, and cyclohexane were supplied by Sinopharm Chemicals Reagent (China). Stock solutions of cerium nitrate were prepared in distilled water and were diluted with distilled water as required and pH adjustment was made using nitric acid.

2.2. Equipments

Infrared spectra of the samples were obtained using a Fourier transform infrared spectrometer in the

frequency range of 400–4,000 cm^{-1} (Nicolet AVATAR360 FTIR System). The surfaces morphologies of the samples were observed by scanning electron microscopy (SEM) (HITACHI SU8010 SEM). Samples were gold coated prior to SEM observation. The specific surface area, pore size, and volume of the material were evaluated by the nitrogen gas adsorption method, with a heating rate of 10 $^{\circ}\text{C min}^{-1}$. N_2 adsorption–desorption experiments were performed at 77 K with an Automatic Volumetric Sorption Analyzer (ASAP2020, TSI, America), employing multipoint Brunauer–Emmett–Teller (BET) isotherm adsorption data fitting. The pH measurement was made by a digital pH meter (shanghai, model SX-620 pH meter). Solution concentrations were measured by Inductively Coupled Plasma Mass Spectrometry, Perkin Elmer Elan DRC-e.

2.3. Synthesis of Materials

Fig. 1 represents our procedure for preparation of poly(allylamine)/silica composite. The initial step involved washing silica with hydrochloric acid to remove possible contaminants. The silica after acidification, silane coupling agent, deionized water, and cyclohexane were placed in a three neck round-bottom flask equipped with an overhead stirrer. After 24 h, the reaction was stopped by filtering off the unreacted cyclohexane. Afterwards, poly(allylamine), deionized water, and methanol were added to the reaction flask. The contents were stirred and degassed under vacuum for 15 min and then heated to 343 K for 48 h. The reaction mixture was cooled, allowed to settle, and then the polymer was carefully decanted. The silicas grafted were mixed with a reagent solution of hydrochloric acid and phosphorus acid in a flask equipped with an overhead stirrer. The flask was heated to 363 K, and formaldehyde solution was gradually added with stirring. The reaction mixture was heated at 363 K for 24 h. The flask was cooled and the product was filtered. The resulting composite was washed and dried to a constant mass at 353 K.

2.4. Batch study for Ce(III) adsorption using the poly(allylamine)/silica composite

To study the effect of contact time on kinetics, the rate of Ce(III) adsorption by the poly(allylamine)/silica composite from aqueous solution was carried out to determine the optimum time required to reach equilibrium [13]. Equilibrium test was determined by shaking of 100 mg L^{-1} Ce(III) with the poly(allylamine)/silica composite vs. liquid ratio of 1 g 50 mL^{-1}

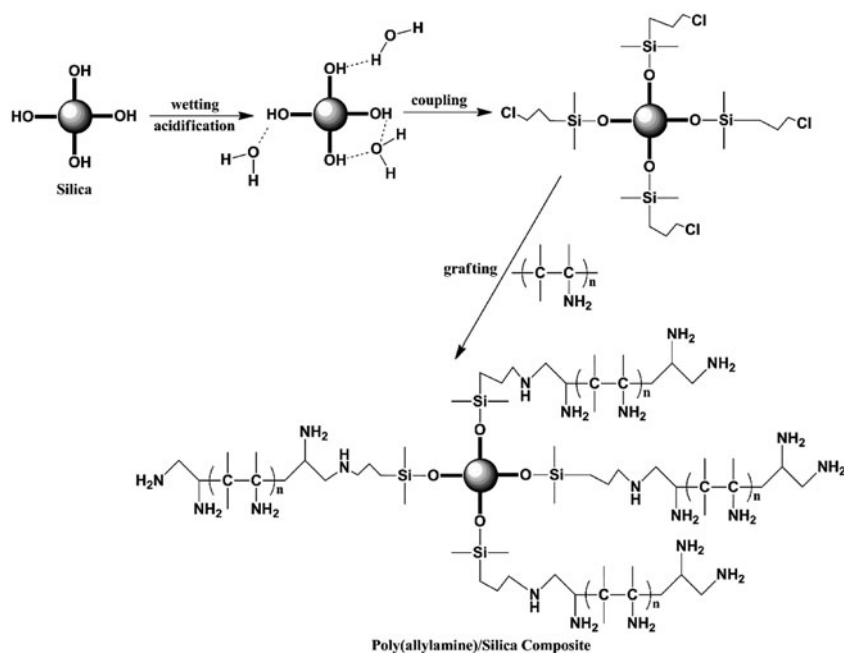


Fig. 1. Proposed mechanistic pathway for synthesis of poly(allylamine)/silica composite.

for varying times from 0 to 200 min at 298 K. For determining the poly(allylamine)/silica composite loading effect, the poly(allylamine)/silica composite loading was varied from 0.02 to 0.20 g 50 mL⁻¹. The poly(allylamine)/silica composite and liquid were then shaken for 3 h at 298 K and Ce(III) concentration 100 mg L⁻¹. Moreover, to study the effect of initial Ce(III) concentration and adsorption isotherm, batch adsorption was conducted by varying the initial Ce(III) concentration of 100–1,000 mg L⁻¹ with the poly(allylamine)/silica composite vs. liquid ratio of 1 g 50 mL⁻¹ for 3 h at 298 K. Effect of pH was also studied by varying the initial pH solution from 1 to 5. At the poly(allylamine)/silica composite/liquid ratio of 1 g 50 mL⁻¹ and Ce(III) concentration of 100 mg L⁻¹, batch adsorption was conducted for 3 h at 298 K.

2.5. Thermodynamics study

Temperature of adsorption isotherms was studied at 298, 308, and 318 K. A 50 mL of cerium nitrate solution at concentration of 100 mg L⁻¹ was equilibrated with 0.2 g the poly(allylamine)/silica composite for 3 h.

3. Theory

3.1. Equilibrium studies

The amount of contaminant absorbed from the aqueous solution is expressed as Ce(III) adsorption

capacity per unit mass of the poly(allylamine)/silica composite q (mg g⁻¹) as:

$$q = \frac{(c_0 - c_e)V}{m} \quad (1)$$

The percentage of Ce(III) removal efficiency Q (%) from the aqueous solution is then calculated from:

$$Q(\%) = \frac{(c_0 - c_e)}{c_0} \times 100\% \quad (2)$$

3.2. Kinetic data analysis

Four kinetic models, i.e. pseudo-first-order, pseudo-second-order, Bangham, Elovich and intraparticle diffusion, were used in order to investigate the adsorption process of Ce(III) onto the adsorbents. The data were processed and fitted to kinetic equations.

First, the pseudo-first-order is the equation used commonly to describe adsorption and it is determined by the following Eq. (3):

$$\frac{dq_t}{dt} = k_1(q_e - q_t) \quad (3)$$

The equation can be integrated by applying boundary conditions $q_t=0$ at $t=0$ and $q_t=q_t$ at $t=t$ [14,15], the equation becomes:

$$\ln(q_e - q_t) = \ln q_e - k_1 t \quad (4)$$

The pseudo-second-order model can be expressed in the form:

$$\frac{dq_t}{dt} = k_2(q_e - q_t)^2 \quad (5)$$

after integrating and applying boundary conditions $q_t=0$ at $t=0$ and $q_t=q_t$ at $t=t$, linear equation form can be obtained:

$$\frac{t}{q_t} = \frac{1}{k_2 q_e^2} + \frac{1}{q_e} t \quad (6)$$

the initial sorption rate, h ($\text{mg g}^{-1} \text{min}^{-1}$) as $t \rightarrow 0$ can be defined as:

$$h = k_2 q_e^2 \quad (7)$$

The initial adsorption rate (h), the equilibrium adsorption capacity (q_e), and the pseudo-second-order constant k_2 can be determined experimentally from the slope and intercept of the plot of t/q_t vs. t [15].

Bangham equation was used to study the step occurring in the present adsorption system [16] and the equation is represented below:

$$\log \log \left[\frac{c_0}{c_0 - q_t m} \right] = \log \left[\frac{k_0 m}{2.303 V} \right] + \alpha_B \log t \quad (8)$$

The Elovich equation assumes that the actual solid surfaces are energetically heterogeneous. The Elovich equation can be expressed as:

$$\frac{dq_t}{dt} = \alpha e^{-\beta q_t} \quad (9)$$

Integrating Eq. (10) and applying the initial conditions $q_t=0$ at $t=0$ and $q_t=q_t$, we get the Elovich model

$$q_t = (1/\beta) \ln(\alpha\beta) + (1/\beta) \ln t \quad (10)$$

where α ($\text{mg g}^{-1} \text{min}^{-1}$) is the initial adsorption rate and the parameter β (g mg^{-1}) is related to the extent of surface coverage and activation energy [17].

Intraparticle diffusion study was also used in this kinetic study. The formula of intraparticle model is presented below:

$$q_t = k_{id} t^{1/2} + c \quad (11)$$

A plot of q_t vs. $t^{1/2}$ should be a straight line with a slope k_{id} and intercept c when adsorption mechanism follows the intraparticle diffusion process. The values of the intercepts give an indication about the thickness of the boundary layer, i.e. the larger the intercept the greater is the boundary layer effect [16,17].

3.3. Adsorption isotherm data analysis

An adsorption isotherm is characterized by certain constant values that represent surface characteristics, affinity of the adsorbent, and adsorption capacity of the adsorbent. To describe the equilibrium of adsorption, various isotherm equations have been applied such as Langmuir, Freundlich, and Tempkin models.

Langmuir adsorption isotherm model assumes that sorption takes place at specific homogeneous sites within the adsorbent and a uniform distribution of energetic adsorption sites. As a consequence, once the adsorbate molecule occupies a site, no more sorption can take place [18].

Therefore, Langmuir model is valid for monolayer adsorption onto a surface with finite number of identical sites [18]. Langmuir parameters were determined by the following formula:

$$q = \frac{q_{\max} K_L C_e}{1 + K_L C_e} \quad (12)$$

The linearization of Eq. (12) is given by Eq. (13) for Langmuir data fitting.

$$\frac{C_e}{q} = \frac{1}{K_L q_{\max}} + \frac{1}{q_{\max}} C_e \quad (13)$$

Furthermore, Freundlich model assumes a heterogeneous surface with a non-uniform distribution of heat of adsorption over the surface and binding sites are not equivalent and/or independent [19]. Freundlich parameters were determined by the formula:

$$q = K_F C_e^{1/n} \quad (14)$$

The linearization of Eq. (14) is given by Eq. (15) for Freundlich data fitting.

$$\log q = \log K_F + \frac{1}{n} \log C_e \quad (15)$$

Tempkin isotherm model considers the interaction between adsorbing species and adsorbate [20]. This model assumes that the heat of adsorption of all the molecules in the layer decreases linearly with coverage due to adsorbate–adsorbent interactions and adsorption is characterized by a uniform distribution of binding energies, up to some maximum binding energy [21]. Tempkin parameters are determined by the formula:

$$q_e = \frac{RT}{b} \ln(K_T C_e) \quad (16)$$

The linear form of Eq. (16) is:

$$q_e = B_1 \ln K_T + B_1 \ln C_e \quad (17)$$

$$B_1 = \frac{RT}{b}$$

where A plot of q_e vs. $\ln C_e$ enables the determination of the isotherm constants K_T and B_1 [22].

3.4. Thermodynamic data analysis

Thermodynamic data such as enthalpy (ΔH°), free energy change or adsorption energy (ΔG°), and entropy (ΔS°) can be obtained from Langmuir or Tempkin constants [16,23]. Adsorption energy formula is:

$$\Delta G^\circ = -RT \log K \quad (18)$$

The equation that expresses the temperature dependence of the adsorption energy is:

$$d\left(\frac{\Delta G^\circ}{T}\right) = -\frac{\Delta H^\circ}{T^2} dT \quad (19)$$

substituting Eq. (18) into Eq. (19) yields:

$$\frac{d \ln K}{d(1/T)} = \frac{-\Delta H^\circ}{RT^2} \quad (20)$$

It assumes that ΔH° is approximately independent of temperature, the slope of $\ln K$ vs. $1/T$ plot result in ΔH° .

If the process is endothermic ($\Delta H^\circ > 0$), the equilibrium constant increases with temperature, whereas if the process is exothermic ($\Delta H^\circ < 0$), the equilibrium constant decreases as temperature is raised.

The change of adsorption entropy can be determined by:

$$\Delta G^\circ = \Delta H^\circ - T\Delta S^\circ \quad (21)$$

4. Results and discussion

4.1. Characteristics of poly(allylamine)/silica composite

4.1.1. FTIR analysis

The spectra of silica and poly(allylamine)/silica composite are presented in Fig. 2, where the curve *a* and curve *b* are the FTIR spectra of silica and poly(allylamine)/silica composite, respectively. The main differences between the two FTIR spectra are 3,320 and 3,150 cm^{-1} corresponding to the stretching vibrations of $-\text{NH}_2$. The bands at 2,960 and 1,410 cm^{-1} corresponding to the stretching vibrations of the ring C–H bonds of modifier and 1,260 cm^{-1} reflects the stretching vibrations of P=O in curve *b*. This observation provides evidence that the modifiers have grafted onto the surface of silica.

4.1.2. SEM analysis

SEM images of silica and poly(allylamine)/silica composite are presented in Fig. 3. As seen from the Fig. 3(a) and (b), the surface of silica is smooth and the particles agglomerate into a larger particle. From the Fig. 3(c) and (d), we can see that the surface of material become rough after modification and there are many lumps attaching on the surface. This should be beneficial for the adsorption of Ce(III). The surface attachments were modifiers that graft onto the surface

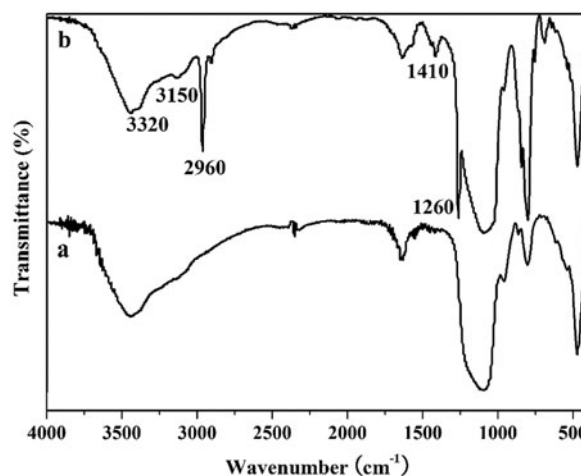


Fig. 2. FTIR spectra of silica (a) and poly(allylamine)/silica composite (b).

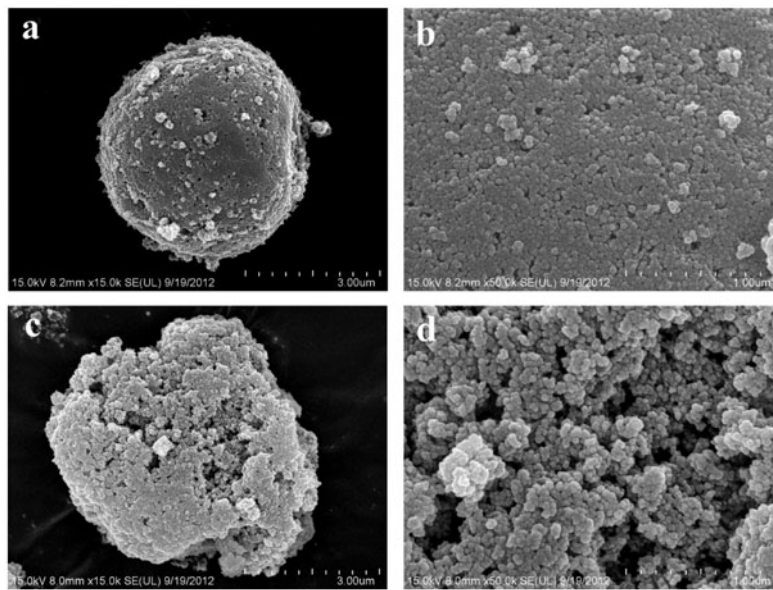


Fig. 3. SEM micrographs of silica (a)×15,000, (b)×50,000 and poly(allylamine)/silica composite (c)×15,000, (d) ×50,000.

of silica, which also would help to improve the adsorption rate because that the functional groups of modifiers formed bond easily with Ce(III).

4.1.3. BET analysis

The location of the hysteresis loop in the N_2 isotherm can be used to determine whether the material possesses a regular framework pore or an interparticle void, such as a textural pore [24]. The silica shows (Fig. 4(b)) well pore size distribution with pore

diameter of 21.47 nm, high surface area ($198 \text{ m}^2 \text{ g}^{-1}$), and high pore volume ($0.43 \text{ cm}^3 \text{ g}^{-1}$) (Fig. 4(b)). Moreover, the framework porosity in the N_2 isotherm indicates the porosity contains within the uniform channels of the template framework. As shown in Fig. 4(a), poly(allylamine)/silica composite appears the presence of both framework porosity and textural porosity which indicated the regular pore size distribution. A decrease in the surface area and pore volume in the composite materials provides further evidence that the poly(allylamine) is embedded inside the pore of the silica.

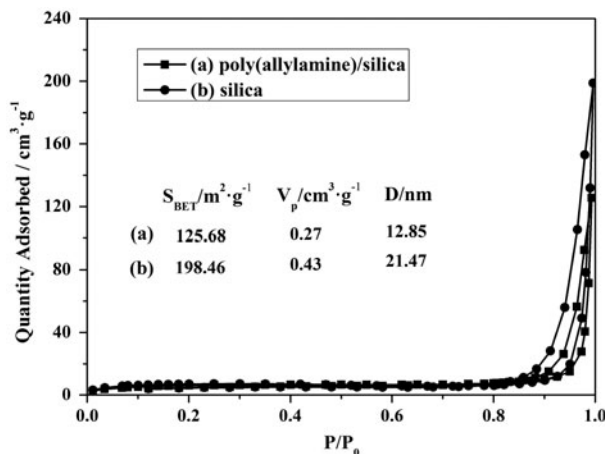


Fig. 4. N_2 adsorption/desorption isotherms of (a) poly(allylamine)/silica composite and (b) silica with the difference of surface areas, pore volumes, and pore sizes.

4.2. Adsorption of Ce(III) using poly(allylamine)/silica composite

In batch experiments, effect of contact time, poly(allylamine)/silica composite loading, initial concentration, pH, and temperature was examined using a synthetic cerium nitrate solution.

4.2.1. Effect of contact time

Fig. 5 shows that Ce(III) adsorption rate increases in the initial 40 min and then significantly slows down. This might be due to the fact that there were abundant vacant adsorbent sites existing originally and the solute gradient was very high. With the progress of adsorption, the Ce(III) adsorption rate composite decreased significantly due to decrease in adsorption sites.

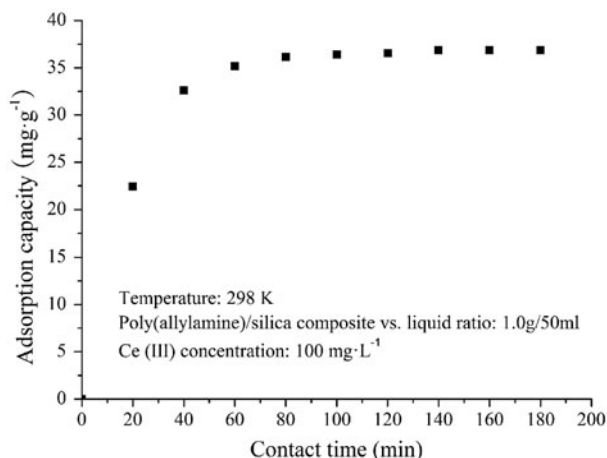


Fig. 5. Effect of contact time on Ce(III) adsorption capacity.

The Ce(III) adsorption on the poly(allylamine)/silica composite could be mainly attributed to the functional groups on the surface of the poly(allylamine)/silica composite which was modified by poly(allylamine) and phosphorous acid. Therefore, it is the coordinate bond which make the poly(allylamine)/silica composite to have the ability to absorb Ce(III).

4.2.2. Effect of adsorbent loading

Fig. 6 shows that the Ce(III) adsorption capacity decreases rapidly with an increasing in the poly(allylamine)/silica composite loading but levels off and achieves equilibrium as the poly(allylamine)/silica composite loading is further increased. This was because the initial Ce(III) concentration was constant

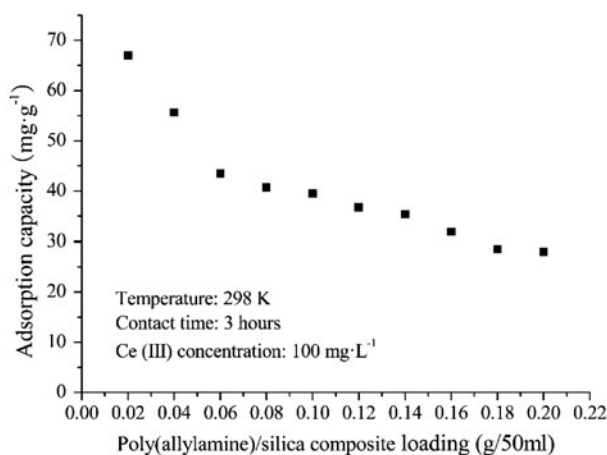


Fig. 6. Effect of poly(allylamine)/silica composite loading on Ce(III) adsorption capacity.

at various amounts of the poly(allylamine)/silica composite loading. Hence, when the Ce(III) was chelated completely with the amino groups on the surface at a certain amount of the poly(allylamine)/silica composite loading, the Ce(III) adsorption reached equilibrium.

4.2.3. Effect of initial Ce(III) concentration

Fig. 7 shows the effect of initial Ce(III) concentration on adsorption capacity of the poly(allylamine)/silica composite increases with increasing initial Ce(III) concentration. It was found that it was positively correlated. This was because the higher initial Ce(III) concentration provided a greater driving force for overcoming mass transfer resistances [25]. As a result, more Ce(III) could migrate from the external surface to the internal micropores of the poly(allylamine)/silica composite within a given contact time [26]. The Ce(III) could be absorbed either on the external surface of poly(allylamine)/silica composite or on its internal surface. The equilibrium was reached when all the Ce(III) and amino group, on the external and internal surfaces of the poly(allylamine)/silica composite, were chelated.

4.2.4. Effect of pH

It is well known that the solution pH is an important factor controlling the surface charge of the adsorbent and the degree of ionization of the adsorbate in aqueous solution [27]. The effect of pH on adsorption capacity of poly(allylamine)/silica composite was investigated over the pH range from 1.0 to 5.0 and the pH dependence of the adsorption performances to

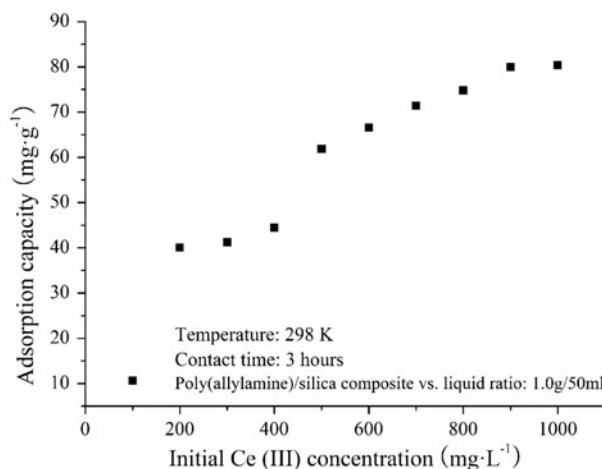


Fig. 7. Effect of initial Ce(III) concentration on Ce(III) adsorption capacity of the poly(allylamine)/silica composite.

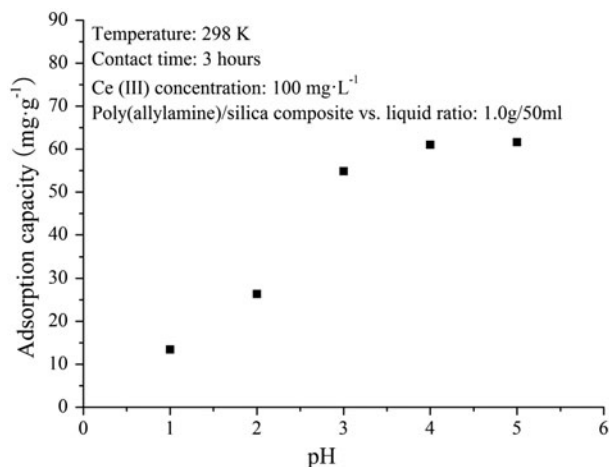


Fig. 8. Effect of pH on Ce(III) adsorption capacity of the poly(allylamine)/silica composite.

Ce(III) is illustrated in Fig. 8. It is found that the adsorption capacity increases with increasing solution pH, and the maximum uptake of Ce(III) occurs at initial pH of 5.0. Similar trend was also observed in many earlier works [28,29]. Therefore, all the adsorption experiments were carried out at pH 5.0. The increasing in Ce(III) adsorption as the pH increases could be explained on the basis of decrease in competition between protons and metal cations for the same functional groups and decrease in the positive surface

charge on the poly(allylamine)/silica composite resulting in a lower electrostatic repulsion between its surface and Ce(III) [30,31]. The low level of Ce(III) uptake at pH below 3.0 might be explained on the basis of the overall surface charge on the poly(allylamine)/silica composite become positive and active sites being protonated, which would inhibit the approach of positively charged metal cations.

4.3. Adsorption kinetics of Ce(III)

The adsorption kinetics of Ce(III) is of critical importance for the design of practical treatment systems. Four kinetic models, pseudo-first-order, pseudo-second-order, Evolich, and Bangham models, were used to fit the experimental data. These kinetic models can also provide the information about the adsorption mechanism.

The pseudo-first-order model, Eq. (4) was used to analyze the experimental data. Fig. 9(a) presents pseudo-first-order kinetic plots for adsorption of Ce(III), and the relevant constants are listed in Table 1. The experimental q_e values were not in agreement with the calculated values using pseudo-first-order kinetics.

The pseudo-second-order model using Eq. (6) also indicated a higher adsorption rate from the value of h and k_2 . Fig. 9(b) shows pseudo-second-order kinetic plots for absorbing of Ce(III). As shown in Table 1, it

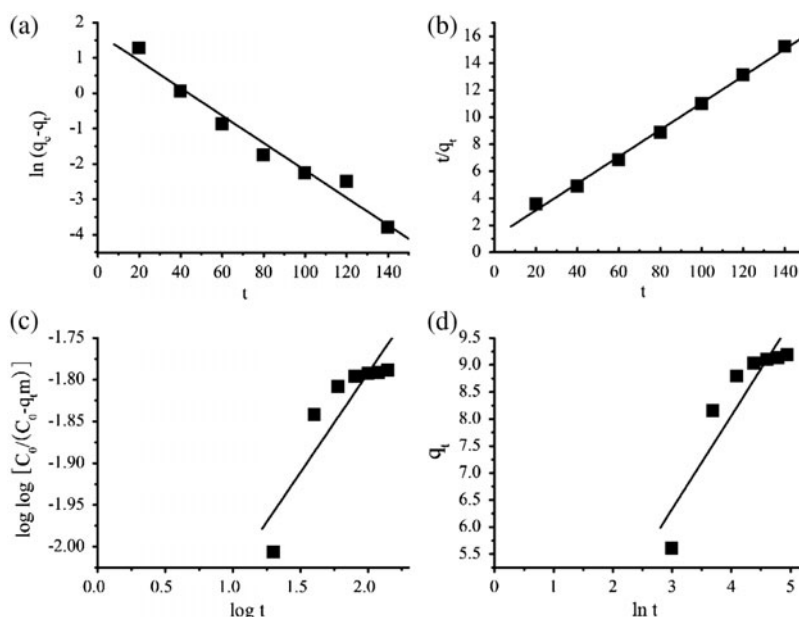


Fig. 9. (a) Pseudo-first-order; (b) Pseudo-second-order; (c) Bangham; (d) Elovich kinetic plots for Ce(III) adsorption by the poly(allylamine)/silica composite.

Table 1
Kinetic parameters for Ce(III) adsorption using kinds of kinetic models

Kinetic models	Parameters			
Pseudo-first-order	$q_{e \text{ exp}}$ (mg g^{-1})	k_1 (min^{-1})	q_e (mg g^{-1})	R^2
	10.7	0.039	5.5	0.97
Pseudo-second-order	h ($\text{mg g}^{-1} \text{min}^{-1}$)	k_2 ($\text{g mg}^{-1} \cdot \text{min}^{-1}$)	q_e (mg g^{-1})	R^2
	0.889	0.00878	10.1	0.99
Bangham		k_0 (mL L g^{-1})	α_B	R^2
		3.109	0.238	0.90
Elovich		α ($\text{mg g}^{-1} \text{min}^{-1}$)	β (g mg^{-1})	R^2
		3.368	0.579	0.91

is worthwhile to note that the calculated adsorption capacities at 100 mg L^{-1} initial Ce(III) concentration is very close to the experimental results in Fig. 7 and the correlation coefficient $R^2 = 0.99$ indicates the applicability of this model for the adsorption data, which indicates the pseudo-second-order model is well fitted with the experimental data of Ce(III) adsorption by the poly(allylamine)/silica composite as compared with the pseudo-first-order model.

Bangham Eq. (8) was used to study the steps occurring in the present adsorption system. Fig. 9(c) presents Bangham kinetic plots for adsorption of Ce(III) by the poly(allylamine)/silica composite. As shown in Table 1, the correlation coefficient $R^2 = 0.90$ indicates the applicability of Bangham model for the adsorption data. The correlation coefficient was lower than other models indicating that the Bangham model fitted no better with the experimental data of the poly(allylamine)/silica composite.

Elovich Eq. (10) was used to study the steps occurring in the present adsorption system. Fig. 9(d) shows Elovich kinetic plots for adsorption of Ce(III) on the poly(allylamine)/silica composite. The R^2 values are not very high in this kinetic model. The regression analysis showed that the Elovich model may not fit very well for the adsorption of Ce(III) of the poly(allylamine)/silica composite.

To sum up, the values of kinetic parameters for all four kinetic models are summarized in Table 1. It is obvious that the pseudo-second-order is the best kinetic model with a satisfactorily fit to kinetic data at 100 mg L^{-1} Ce(III) concentrations.

4.4. Intraparticle diffusion model

Intraparticle diffusion model is used to analyze the experimental data. This model is effective when a multistep process occurs during adsorption. Each step can be identified by a change of the slope of the linear line used to fit the experimental data. Using the plot

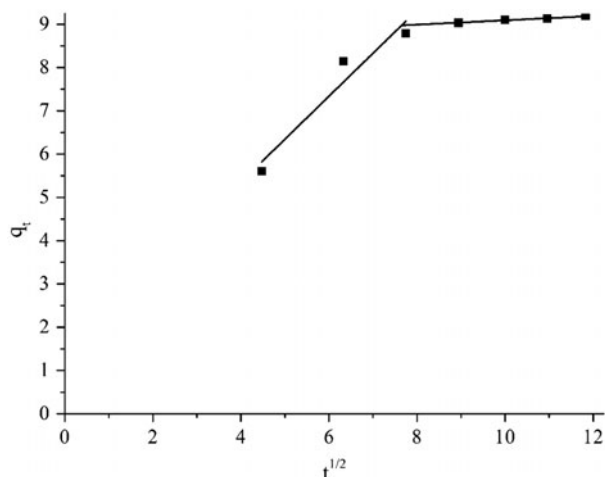


Fig. 10. Intraparticle diffusion plots for Ce(III) adsorption.

of q_t vs. $t^{1/2}$ of Eq. (11), the experimental data in this study show two separate regions (see Fig. 10). Two regions corresponding with two different steps in the adsorption process were identified. The initial region would correspond to the external diffusion, whereas the final part would be due to the intraparticle diffusion. Therefore, Fig. 10 implied that during the adsorption process, there was a fast diffusion for adsorption onto the external surface followed by a very slow diffusion onto the internal surface. This was likely due to at high ionic strengths in external and a decrease of the poly(allylamine)/silica composite hole radius in internal. Meanwhile, the straight line did not pass through the origin. These findings suggested that the intraparticle diffusion was not the only rate-controlling mechanism in the Ce(III) adsorption process.

4.5. Adsorption isotherm

An adsorption isotherm can be characterized by Langmuir, Freundlich, and certain constants that

represent the surface characteristics, the affinity of the adsorbent, and the adsorption capacity of the adsorbent. During this research, three isotherm models were tested to find the most appropriate correlation of the experimental equilibrium curves. Such an adsorption isotherm is very important for the designing of an adsorption system.

In the present work, the monolayer capacity, q_{\max} calculated using Eq. (13) is found to be 109.3 mg g^{-1} at initial Ce(III) concentrations of $100\text{--}1,000 \text{ mg L}^{-1}$. Meanwhile, the experimental adsorption capacity q_{exp} is 111.8 mg g^{-1} (see Table 2). Theoretical q_{\max} value calculated from this model was in good agreement with the experimental Ce(III) adsorb capacity. Fig. 11(a) presents the linearized Langmuir adsorption isotherm of Ce(III) curve. The correlation coefficient $R^2=0.95$

indicates the applicability of Langmuir isotherm for the adsorption data. The correlation coefficient showed that the Langmuir isotherm almost fitted with the experimental data of the poly(allylamine)/silica composite.

The Freundlich equation is used to describe heterogeneous adsorption systems and n reflected the adsorption intensity. The experimental data were examined using Eq. (15). Fig. 11(b) shows the linearized Freundlich adsorption isotherm of Ce(III) curve and the Freundlich parameters are presented in Table 2. Similar values of $1/n$ which were less than 1 had been reported for Ni (II) removal using resin [32]. The n value of 1.773 meant that the adsorption system of Ce(III) using the poly(allylamine)/silica composite contained adsorption onto the external surface and

Table 2
Adsorption isotherms constants

Isotherm models	Parameters			
Langmuir	$q_{\text{exp}} (\text{mg g}^{-1})$	$q_{\max} (\text{mg g}^{-1})$	$K_L (\text{L mg}^{-1})$	R^2
Freundlich	111.8	109.3	0.00467	0.95
	$K_F (\text{mg g}^{-1})/(\text{mg L}^{-1})^{1/n}$		$n (\text{mg L}^{-1})$	R^2
Tempkin	2.376		1.773	0.97
	$K_T (\text{L mg}^{-1})$		$B_1 (\text{J mol}^{-1})$	R^2
	0.0339		21.044	0.92

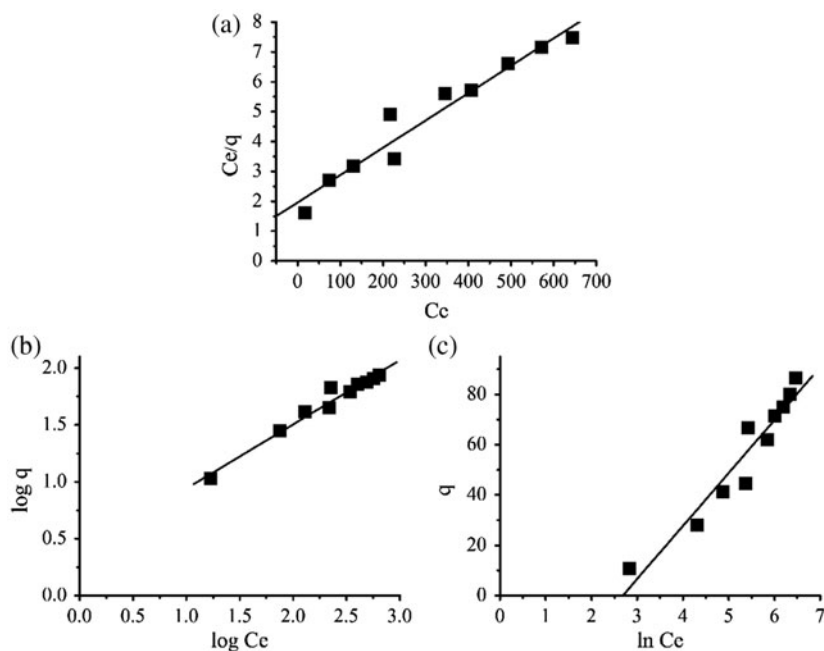


Fig. 11. (a) The linearized Langmuir, (b) Freundlich, and (c) Tempkin adsorption isotherm of Ce(III) curve.

diffusion onto the internal surface. The correlation coefficient $R^2 = 0.97$ indicated the applicability of Freundlich isotherm for the adsorption data. The correlation coefficient was higher than the Langmuir model which showed that the Freundlich isotherm fitted better with the experimental data of the poly(allylamine)/silica composite.

Tempkin isotherm equation assumes that the heat of adsorption of all the molecules in the layer decreases linearly with the coverage of molecules due to the adsorbent–adsorbate repulsions. The adsorption of adsorbate is uniformly distributed and that the fall in the heat of adsorption is linear than logarithmic. The experimental data were examined using Eq. (17). The Tempkin parameters are presented in Table 2 and the linearized Tempkin adsorption isotherm of Ce(III) curve is shown in Fig. 11(c). It could be found that adsorption of Ce(III) on poly(allylamine)/silica composite was mainly via chemical adsorption from the value of B_1 . But the correlation coefficient was lower indicating that the Tempkin isotherm did not fit better with the experimental data of the poly(allylamine)/silica composite.

To sum up, the experimental data are best fitted by the Freundlich model which can be seen from the high value of the correlation coefficient ($R^2 = 0.97$) in Table 2. However, other studies have reported that the adsorption isotherm of metal ions removal using other adsorption materials could be more generically approximated by the Langmuir model [32,33]. In this study, the fact that the data fit no better with the Langmuir model than other two models indicate that the poly(allylamine)/silica composite has a heterogeneous surface with a non-uniform distribution of heat of adsorption over the surface.

4.6. Thermodynamic study

Thermodynamic parameters such as enthalpy (ΔH°), free energy change or adsorption energy (ΔG°), and entropy (ΔS°) are obtained in this study from Langmuir constant under various temperatures (298, 308, and 318 K) using Eqs. (18), (20), and (21) [33–35].

Fig. 12 shows the experimental results of temperature effect on the adsorption isotherm determined using the isotherm of Ce(III) on the poly(allylamine)/silica composite under the temperatures of 298, 308, and 318 K. It can be seen that the adsorption capacity increases with the increase of temperature. Langmuir isotherm constants for Ce(III) adsorption on the poly(allylamine)/silica composite is presented in Table 3. The effect of temperature on K may be used to calculate ΔG° using Eq. (18) and the K value in Eq. (18) must be dimensionless. Then K can be

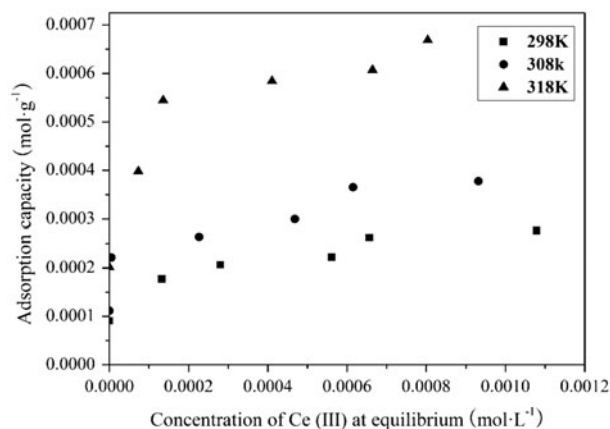


Fig. 12. Effect of temperature on the exchange isotherm of Ce(III).

Table 3

Langmuir isotherm constants for Ce(III) adsorbed on the poly(allylamine)/silica composite

T (K)	Langmuir models		
	q_{\max} (mmol g ⁻¹)	K_L' (L mol ⁻¹)	R^2
298	0.283	14,559.62	0.98
308	0.378	24,752.75	0.98
318	0.663	32,063.90	0.99

recalculated as dimensionless by multiplying it with 55.5 (number of moles of water per liter of solution) [36] and the results are shown in Table 4. According to Liu [37], the Gibbs free energy change could be calculated using Langmuir equilibrium constant and it was reasonable for a dilute solution of a charged adsorbate except for multivalent cation adsorbate. The results showed that the adsorption process was spontaneous this is indicated by the negative value of ΔG° . It was interesting to note that the higher temperature had more negative value which meant that the higher temperature provided more energetically favorable adsorption.

Table 4

ΔG° values for adsorption of Ce(III) on the poly(allylamine)/silica composite at various temperatures

T (K)	K	ΔG° (kJ mol ⁻¹)
298	808,058.91	-33.70
308	1,373,777.63	-36.19
318	1,779,546.45	-38.05

As ΔH° was approximately independent of temperature over narrow temperature range, from Eq. (20) the slope of $\ln K$ vs. $1/T$ plot could be used to determine ΔH° . ΔH° of adsorption was obtained as $71.87 \text{ kJ mol}^{-1}$. The positive value of ΔH° indicated the endothermic nature of adsorption process. This was in agreement with the expected higher negative values of ΔG° at a higher temperature for endothermic adsorption. The change of adsorption entropy was determined using Eq. (21). ΔS° was calculated at 298 K as $0.502 \text{ kJ mol}^{-1} \text{ K}^{-1}$. The positive value of ΔS° suggested the increased randomness at the solid–solution interface during adsorption.

4.7. Reversibility and reusability

In this study, adsorption experiments were performed using 1 g poly(allylamine)/silica composite and 50 mL of 100 mg L^{-1} Ce(III) at 298 K for 120 min, and desorption of adsorbed Ce(III) onto poly(allylamine)/silica composite was studied using 2 mol L^{-1} HCl, with poly(allylamine)/silica composite/liquid ratio of $1 \text{ g } 10 \text{ mL}^{-1}$ for 30 min, and consecutive adsorption–desorption cycles were repeated eight times. The results are shown in Table 5. There was a slight decrease with the increase of cycle times in adsorption efficiency from 111.8 mg g^{-1} for the first cycle to 98.66 mg g^{-1} for the eighth cycle. The poly(allylamine)/silica composite that was regenerated by eight cycles in HCl solution had high Ce(III) removal efficiency with its adsorption efficiency of 98.66 mg g^{-1} .

4.8. Effect of competing ions in Ce(III) sorption

The Ce(III) can substitute by other cation due to similar ionic radius [38,39]. Therefore, the presence of several co-existing cations may affect the Ce(III) sorption and reduce the efficiency of the poly(allylamine)/silica composite. Then the experiments were carried out the possible interfering of 10-fold concentration of Al(III), Ca(II), Na(I). The data of decreasing amount uptakes in Table 6. The presence of Ca(II) and Na(I) did not significantly affect Ce(III) sorption by the poly

Table 6

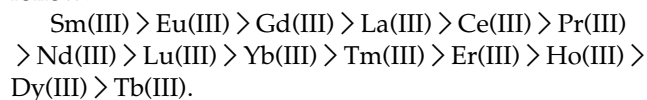
Ce(III) sorption inhibition in the presence of competing cations by poly(allylamine)/silica composite

Competing cations	Ce(III) Sorption decrease (%)
Al(III)	26.66
Ca(II)	3.22
Na(I)	0.16

(allylamine)/silica composite. However, the Ce(III) sorption was markedly affected by the presence of Al(III). This was probably the similar ionic charge of Ce(III) and Al(III). In the presence of 10-fold Al(III), the sorption capacity of Ce(III) decreased 22.66%, which is greater than two thirds of the sorption capacity without Al(III) interfering. This was probably the similar ionic charge of Ce(III) and Al(III) [24].

4.9. Intra-series adsorption behavior of lanthanide element

To determine the intra-series adsorption behavior of lanthanide element of the poly(allylamine)/silica composite, 1 g adsorbent was tested under each rare earth ion concentration of 20.0 mg L^{-1} in the 50 mL solution. The selectivity order of poly(allylamine)/silica composite among lanthanide element cations follow:



The change presented in intra-series adsorption behavior of lanthanide element because that series of lanthanide elements filled electron only inner 4f orbit with the increase of atomic number. There was same electron configuration in their outer orbit, which led to the similar chemical properties within the series. The ionic radius of lanthanide elements decreased with the increase of atomic number due to the lanthanide contraction. The adsorption quantity of the lanthanum rare earth ions on poly(allylamine)/silica composite showed different change order based on the above reasons.

Table 5

Data about reversibility and reusability of poly(allylamine)/silica composite

No. of cycles	1	2	3	4	5	6	7	8
Ce(III) adsorption capacity/ mg g^{-1}	111.8	109.9	108.0	106.9	105.3	103.2	100.1	98.66

5. Conclusion

The poly(allylamine)/silica composite was prepared successfully through a coupling reaction followed by a “graft-to” method. From the results of FTIR and SEM in this research, it could be concluded that the poly(allylamine)/silica composite was suitable to adsorb Ce(III). The adsorption kinetics was best approximated by the pseudo-second-order model. The adsorption isotherm results indicated that Freundlich model provided the best fit for the equilibrium data. Thermodynamic parameters were also determined in this study. The negative value of ΔG° indicated the spontaneous nature of the adsorption process. The adsorption process was found to be endothermic which was confirmed by the positive sign of ΔH° . ΔS° was positive indicating the increasing randomness at the solid–solution interface during adsorption. There was a slight decrease with the increase of cycle times in adsorption efficiency (111.8 mg g⁻¹ for the first cycle and 98.66 mg g⁻¹ for the eighth cycle). In the presence of monovalent and divalent competing ions, the sorption was not adversely affected by the poly(allylamine)/silica composite. However, the presence of trivalent Al(III) was sharply decreased the Ce(III) sorption capacity. The intra-series adsorption behavior about lanthanide element of the poly(allylamine)/silica composite was different. Considering very promising data for the adsorption of Ce(III), more works are still required to determine the adsorption performance of poly(allylamine)/silica composite for other REEs since they present the similar chemical and physical behavior with Ce(III), further sorption studies should be performed to take the advantage of this process.

Acknowledgments

This work was supported by Public Service Project of the Chinese Ministry of Land and Resources (201311024).

Abbreviations

q	—	Ce(III) adsorption capacity per unit mass of the modified silica adsorption material (mg g ⁻¹)
C_0	—	initial Ce(III) concentration (mg L ⁻¹)
C_e	—	equilibrium Ce(III) concentration (mg L ⁻¹)
V	—	volume of metal ion solution (L)
m	—	mass of modified silica adsorption material (g)

Q	—	removal efficiency of Ce(III)
q_t	—	amount of adsorbate adsorbed at time (mg g ⁻¹)
t	—	time (min)
q_e	—	equilibrium adsorption capacity (mg g ⁻¹)
k_1	—	rate constant of pseudo-first-order model (min ⁻¹)
k_2	—	rate constant of pseudo-second-order model (g mg ⁻¹ min ⁻¹)
h	—	initial sorption rate (mg g ⁻¹ min ⁻¹)
a_B, k_0	—	bangham constants
α	—	initial adsorption rate (mg g ⁻¹ min ⁻¹)
β	—	parameter related to the extent of surface coverage and activation energy (g mg ⁻¹)
k_{id}	—	intraparticle diffusion rate constant
q_{max}	—	monolayer capacity attained at high concentrations (mg L ⁻¹)
K_L	—	langmuir equilibrium constant (L mg ⁻¹)
K_F	—	freundlich capacity factor (mg g ⁻¹)/(mg L ⁻¹) ^{1/n}
n	—	reciprocal of Freundlich intensity parameter
K_T	—	tempkin equilibrium binding constant (L mol ⁻¹)
B_1	—	heat of adsorption
K	—	equilibrium constant (L mol ⁻¹)
ΔG°	—	gibbs free energy change or adsorption energy (kJ mol ⁻¹)
ΔH°	—	enthalpy change (kJ mol ⁻¹)
ΔS°	—	entropy change (kJ mol ⁻¹ K ⁻¹)

References

- [1] Z. Chen, Global rare earth resources and scenarios of future rare earth industry, *J. Rare Earth* 29 (2011) 1–6.
- [2] H.J. Liu, Static conditions of concentrated Alkali decomposition of Baotou rare earth ore, *Chin. Rare Earths* 32 (2011) 68–71.
- [3] L. Pietrelli, B. Bellomo, D. Fontana, M. Montereali, Rare earths recovery from NiMH spent batteries, *Hydrometallurgy* 66 (2002) 135–139.
- [4] K. Gschneidner Jr., Rare earth speciality inorganic chemicals, in: *Symposium on Speciality Inorganic Chemicals*, The Royal Society of Chemistry, London, 1980, pp. 403–443.
- [5] J. Benedetto, V. Ciminelli, J.D. Neto, Comparison of extractants in the separation of samarium and gadolinium, *Miner. Eng.* 6 (1993) 597–605.
- [6] H. Tokuyama, T. Yoshida, L. He, Preparation of novel emulsion gel adsorbents and their adsorption properties for heavy-metal ions, *Ind. Eng. Chem. Res.* 50 (2011) 10270–10277.

- [7] H. Zhou, L. Yang, W. Li, F. Wang, W. Li, J. Zhao, X. Liang, H. Liu, Immobilizing penicillin G acylase using silica-supported ionic liquids: The effects of ionic liquid loadings, *Ind. Eng. Chem. Res.* 51 (2012) 13173–13181.
- [8] K.D. Demadis, E. Mavredaki, M. Somara, Additive-driven dissolution enhancement of colloidal silica. 1. Basic principles and relevance to water treatment, *Ind. Eng. Chem. Res.* 50 (2011) 12587–12595.
- [9] V. Kailasam, E. Rosenberg, Oxyanion removal and recovery using silica polyamine composites, *Hydrometallurgy* 129 (2012) 97–104.
- [10] Q.X. Nguyen, T.G. Belgard, J.J. Taylor, V.S. Murthy, N.J. Halas, M.S. Wong, Water-phase synthesis of cationic silica/polyamine nanoparticles, *J. Chem. Mater.* 24 (2012) 1426–1433.
- [11] J.J. Allen, E. Rosenberg, E. Johnston, C. Hart, Sol–gel synthesis and characterization of silica polyamine composites: Applications to metal ion capture, *ACS Appl. Mater. Interfaces* 4 (2012) 1573–1584.
- [12] Z. Fan, J. Shen, R. Li, S. Li, Synthesis and adsorption behavior of surface Cu (II) ion-imprinted poly(allylamine)-silica gel material, *Polym-Plast. Technol.* 51 (2012) 1289–1295.
- [13] V. Srivastava, C. Weng, V. Singh, Y. Sharma, Adsorption of nickel ions from aqueous solutions by nano alumina: Kinetic, mass transfer, and equilibrium studies, *J. Chem. Eng. Data* 56 (2011) 1414–1422.
- [14] Y.S. Ho, G. McKay, Pseudo-second order model for sorption processes, *Process Biochem.* 34 (1999) 451–465.
- [15] H. Tavakoli, H. Sepehrian, R. Cheraghali, Encapsulation of nanoporous MCM-41 in biopolymeric matrix of calcium alginate and its use as effective adsorbent for lead ions: Equilibrium, kinetic and thermodynamic studies, *J. Taiwan Inst. Chem. E.* 44 (2013) 343–348.
- [16] N. Chen, C. Feng, Z. Zhang, R. Liu, Y. Gao, M. Li, N. Sugiura, Preparation and characterization of lanthanum(III) loaded granular ceramic for phosphorus adsorption from aqueous solution, *J. Taiwan Inst. Chem. E.* 43 (2012) 783–789.
- [17] S. Wang, L. Li, H. Wu, Z. Zhu, Unburned carbon as a low-cost adsorbent for treatment of methylene blue-containing wastewater, *J. Colloid Interface Sci.* 292 (2005) 336–343.
- [18] E. Vaudevire, E. Koreman, G. Galjaard, R. Trommel, M. Visser, Further treatment of highly concentrated brine with dynamic vapour recompression, *Desalin. Water Treat.* 51 (2013) 4958–4962.
- [19] S.M. Xu, S.F. Zhang, R.W. Lu, J.Z. Yang, C.X. Cui, Study on adsorption behavior between Cr(VI) and crosslinked amphoteric starch, *J. Appl. Polym. Sci.* 89 (2003) 263–267.
- [20] C. Duran, D. Ozdes, A. Gundogdu, H.B. Senturk, Kinetics and isotherm analysis of basic dyes adsorption onto almond shell (*Prunus dulcis*) as a low cost adsorbent, *J. Chem. Eng. Data.* 56 (2011) 2136–2147.
- [21] L. Zeng, X. Li, J. Liu, Adsorptive removal of phosphate from aqueous solutions using iron oxide tailings, *Water Res.* 38 (2004) 1318–1326.
- [22] R. Qu, M. Wang, R. Song, C. Sun, Y. Zhang, X. Sun, C. Ji, C. Wang, P. Yin, Adsorption kinetics and isotherms of Ag(I) and Hg(II) onto silica gel with functional groups of hydroxyl- or amino-terminated polyamines, *J. Chem. Eng. Data* 56 (2011) 1982–1990.
- [23] I.D. Mall, V.C. Srivastava, N.K. Agarwal, Removal of Orange-G and Methyl Violet dyes by adsorption onto bagasse fly ash-kinetic study and equilibrium isotherm analyses, *Dyes Pigm.* 69 (2006) 210–223.
- [24] M.R. Awual, T. Kobayashi, H. Shiwaku, Y. Miyazaki, R. Motokawa, S. Suzuki, Y. Okamoto, T. Yaita, Evaluation of lanthanide sorption and their coordination mechanism by EXAFS measurement using novel hybrid adsorbent, *Chem. Eng. J.* 225 (2013) 558–566.
- [25] A. Demir, A. Gunay, E. Debik, Ammonium removal from aqueous solution by ion-exchange using packed bed natural zeolite, *Water SA* 28 (2002) 329–336.
- [26] Q. Du, S. Liu, Z. Cao, Y. Wang, Ammonia removal from aqueous solution using natural Chinese clinoptilolite, *Sep. Purif. Technol.* 44 (2005) 229–234.
- [27] N. Sakkayawong, P. Thiravetyan, W. Nakbanpote, Adsorption mechanism of synthetic reactive dye wastewater by chitosan, *J. Colloid Interface Sci.* 286 (2005) 36–42.
- [28] M.N. Zafar, R. Nadeem, M.A. Hanif, Biosorption of nickel from protonated rice bran, *J. Hazard. Mater.* 143 (2007) 478–485.
- [29] H. Xu, Y. Liu, J.H. Tay, Effect of pH on nickel biosorption by aerobic granular sludge, *Bioresour. Technol.* 97 (2006) 359–363.
- [30] Z. Reddad, C. Gerente, Y. Andres, P. Le Cloirec, Adsorption of several metal ions onto a low-cost biosorbent: Kinetic and equilibrium studies, *Environ. Sci. Technol.* 36 (2002) 2067–2073.
- [31] M. Iqbal, A. Saeed, Production of an immobilized hybrid biosorbent for the sorption of Ni(II) from aqueous solution, *Process Biochem.* 42 (2007) 148–157.
- [32] N. Dizge, B. Keskinler, H. Barlas, Sorption of Ni(II) ions from aqueous solution by Lewatit cation-exchange resin, *J. Hazard. Mater.* 167 (2009) 915–926.
- [33] A. Ma, T. Shek, S. Allen, V. Lee, G. McKay, Removal of nickel from effluents by chelating ion exchange, *J. Chem. Technol. Biotechnol.* 83 (2008) 1623–1632.
- [34] M. Monier, D. Ayad, Y. Wei, A. Sarhan, Adsorption of Cu(II), Co(II), and Ni(II) ions by modified magnetic chitosan chelating resin, *J. Hazard. Mater.* 177 (2010) 962–970.
- [35] M. Addy, B. Losey, R. Mohseni, E. Zlotnikov, A. Vasiliev, Adsorption of heavy metal ions on mesoporous silica-modified montmorillonite containing a grafted chelate ligand, *Appl. Clay Sci.* 59 (2012) 115–120.
- [36] S.K. Milonjić, A consideration of the correct calculation of thermodynamic parameters of adsorption, *J. Serb. Chem. Soc.* 72 (2007) 1363–1367.
- [37] Y. Liu, Is the free energy change of adsorption correctly calculated? *J. Chem. Eng. Data* 54 (2009) 1981–1985.
- [38] M.R. Awual, T. Yaita, H. Shiwaku, Design a novel optical adsorbent for simultaneous ultra-trace cerium (III) detection, sorption and recovery, *Chem. Eng. J.* 228 (2013) 327–335.
- [39] M.R. Awual, T. Kobayashi, Y. Miyazaki, R. Motokawa, H. Shiwaku, S. Suzuki, Y. Okamoto, T. Yaita, Selective lanthanide sorption and mechanism using novel hybrid Lewis base (N-methyl-N-phenyl-1,10-phenanthroline-2-carboxamide) ligand modified adsorbent, *J. Hazard. Mater.* 252 (2013) 313–320.